Inorganic Chemistry
Cite This: Inorg. Chem. 2018, 57, 7259−7269
Article
pubs.acs.org/IC

Solution and Solid State Structural Chemistry of Th(IV) and U(IV) 4-Hydroxybenzoates

Nicole A. Vanagas,[†] Jennifer N. Wacker,[†] Christopher L. Rom,[†] Elliot N. Glass,[‡] Ian Colliard,[‡] Yusen Qiao,[∥] Jeffery A. Bertke,[†] Edward Van Keuren,[§] Eric J. Schelter,[∥] May Nyman,[‡] and Karah E. Knope*[,†]

[†]Department of Chemistry, Georgetown University, 37th and O Streets Northwest, Washington, D.C. 20057, United States
[‡]Department of Chemistry, Oregon State University, Corvallis, Oregon 97331, United States
[§]Department of Physics, Georgetown University, 37th and O Streets Northwest, Washington, D.C. 20057, United States
[∥]P. Roy and Diana T. Vagelos Laboratories, Department of Chemistry, University of Pennsylvania, 231 South 34th Street, Philadelphia, Pennsylvania 19104, United States

Supporting Information

ABSTRACT: Organic ligands with carboxylate functionalities have been shown to affect the solubility, speciation, and overall chemical behavior of tetravalent metal ions. While many reports have focused on actinide complexation by relatively simple monocarboxylates such as amino acids, in this work we examined Th(IV) and U(IV) complexation by 4-hydroxybenzoic acid in water with the aim of understanding the impact that the organic backbone has on the solution and solid state structural chemistry of thorium(IV) and uranium(IV) complexes. Two compounds of the general formula $[An_6O_4(OH)_4(H_2O)_6(4\text{-HB})_{12}]\cdot nH_2O$ [An = Th (**Th-1**) and U (**U-1**); 4-HB = 4-hydroxybenzoate] were synthesized via room-temperature reactions of $AnCl_4$ and 4-hydroxybenzoic acid in water. Solid state structures were determined by single-crystal X-ray diffraction, and the compounds were further characterized by Raman, infrared, and optical spectroscopies and thermogravimetry. The magnetism of **U-1** was also examined. The structures of the Th and U compounds are isomorphous and are built from ligand-decorated oxo/hydroxo-bridged hexanuclear units. The relationship between the building units observed in the solid state structure of **U-1** and those that exist in solution prior to crystallization as well as upon dissolution of **U-1** in nonaqueous solvents was investigated using small-angle X-ray scattering, ultraviolet−visible optical spectroscopy, and dynamic light scattering. The evolution of U solution speciation as a function of reaction time and temperature was examined. Such effects as well as the impact of the ligand on the formation and evolution of hexanuclear U(IV) clusters to UO_2 nanoparticles compared to prior reported monocarboxylate ligand systems are discussed. Unlike prior reported syntheses of Th and U(IV) hexamers where the pH was adjusted to ∼2 and 3, respectively, to drive hydrolysis, hexamer formation with the HB ligand appears to be promoted only by the ligand.

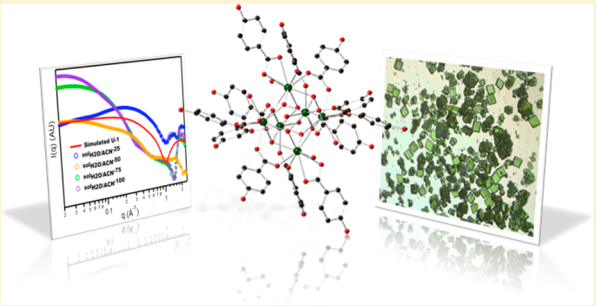

INTRODUCTION

Actinide carboxylates have been intensely investigated over the past few decades because of their relevance to a number of processes, including separation chemistries, waste management, and the environmental behavior of radionuclides.[1] Such work is motivated by a general recognition that the composition, charge, and nuclearity of the species that form and persist in solution or otherwise precipitate into a solid phase have a significant impact on the overall chemical behavior of the actinides. With an eye on the solid state, arguably the most well examined actinide is uranium in its hexavalent oxidation state;[2−4] however, recent work showing the unexpected mobility of tetravalent actinides in environmental systems as well the significance of polynuclear complexes in separations and waste management has fueled efforts investigating the solution and solid state structural chemistry of tetravalent actinide metal ions.[1,5−11]

As compared to the hexavalent actinides, which almost invariably form the well-known actinyl cation (AnO_2^{2+}) under aqueous conditions, the tetravalent actinides adopt more spherical or isotropic coordination geometries, thereby leading to structural units that not surprisingly are quite distinct from those of the hexavalent metal ions.[4,12,13] Moreover, because of their high Lewis acidity, the tetravalent actinides have an increased propensity to hydrolyze and condense to form oligomeric species that further complicate their behavior. Such reactions are governed by the acidity of the metal, its concentration, and solution conditions, including pH, ionic

Received: April 5, 2018
Published: June 7, 2018

DOI: 10.1021/acs.inorgchem.8b00919
Inorg. Chem. 2018, 57, 7259−7269

strength, and temperature.[14,15] It has also been shown that within these systems, the ligands play a critical role either competing with hydrolysis and condensation or otherwise directing the formation of soluble species.[16,17]

Within tetravalent actinide−organic carboxylate ligand systems, a number of structural units have been reported in the solid state. These range in nuclearity from mononuclear complexes to polynuclear species that include di-, tri-, tetra-, hexa-, deca-, dodeca-, hexadeca-, and octatriaconta-nuclear oligomers.[4,6,7,9,10,17−27] Of these species, the hexanuclear units have been observed most frequently, having been prepared across a range of ligand systems and reaction conditions.[12,28] Solution-based techniques, including extended X-ray absorption fine structure (EXAFS), small-angle X-ray scattering (SAXS), and high-energy X-ray scattering (HEXS), have established the presence of the hexamer in solution; however, interestingly for thorium−glycine aqueous systems, wherein solution speciation was elucidated using HEXS, it was found that the assembly of the hexanuclear entity occurred only after the addition of glycine to a solution of dimeric species, suggesting that both the dimeric species and the carboxylate were necessary for assembly of the hexanuclear unit.[16] This work further suggested that the carboxylate played a directing role in the formation of the hexanuclear units.

Inspired by these results, our group is interested in understanding the role that complexing ligands play in templating the self-assembly of An(IV) structural units as well as the effects that the identity of the organic may have on the reactivity of these structural units as a function of solution conditions. In this work, we examined the self-assembly of Th(IV) and U(IV) species in the presence of 4-hydroxybenzoic acid (4-HBA) in aqueous solution. This ligand was chosen for several reasons. (1) It allows us to examine the role that a bulkier, monocarboxylate ligand has on Th(IV) and U(IV) complex formation and reactivity. (2) Its pK_a (4.54) is not overly basic such that it would promote the formation of amorphous hydroxides. (3) It may provide facile crystallization of the solution complexes because of its relatively limited solubility and potential to form supramolecular networks arising from hydrogen bonding and $\pi-\pi$ stacking interactions. From these studies, we obtained $[An_6O_4(OH)_4(H_2O)_6(4\text{-}HB)_{12}]\cdot nH_2O$ [An = Th (**Th-1**) and U (**U-1**); 4-HB = 4-hydroxybenzoate], both at pH <1.5 without added base. To correlate the U(IV) building units observed in the solid state with those in solution prior to precipitation, we employed SAXS and optical absorption spectroscopy. The stability of the cluster cores upon dissolution and the reactivity of the clusters as a function of temperature were also examined to further improve our limited knowledge of the transformation of discrete molecular clusters to nanoparticles.[8] The magnetic and thermal behavior of **U-1** is also presented.

EXPERIMENTAL METHODS

Materials. $ThCl_4$ (International Bioanalytical Industries, Inc.) and 4-hydroxybenzoic acid (99%, Aldrich) were used as received, and UCl_4 was synthesized following published literature procedures.[29] Details of the UCl_4 synthesis are provided as Supporting Information. Nanopure water (≤0.05 μS; Millipore USA) was used in all reactions. To prevent oxidation of U(IV), we employed nanopure water that was boiled and degassed, in addition to the use of a nitrogen-filled glovebox for all synthetic manipulations.

Synthesis. Caution: *^{232}Th and ^{238}U are alpha-emitting radionuclides, and standard precautions for handling radioactive materials should be followed when working with the quantities used in the syntheses that follow.*

Th-1, $Th_6O_4(OH)_4(4\text{-}HB)_{12}(H_2O)_6\cdot 12(H_2O)$, was synthesized at room temperature. $ThCl_4$ (0.075 g, 0.2 mmol) was dissolved in 2 mL of H_2O. The solution was then transferred to a 3 mL shell vial containing 4-hydroxybenzoic acid (0.055 g, 0.4 mmol). The vial was capped, vortexed for <1 min, and then left on the benchtop at room temperature (initial pH of 1.25). Colorless block crystals and white, undissolved ligand were observed after 24 h. After 2 days, a colorless solution (pH 0.90) was decanted and the reaction product was isolated, washed twice with water, and left under ambient conditions to air-dry. We note that efforts to wash away unreacted ligand using ethanol resulted in decomposition of the crystals. Therefore, blocklike crystals of **Th-1** were manually separated from the bulk reaction product (yield of 0.021 g, 18.1% based on Th). The yield of compound **Th-1** was found to increase with reaction time; harvesting the crystals after 3 days resulted in a yield of 44.8% (0.052 g) based on Th. Elemental Anal. Calcd (obs): C, 28.76% (28.57%); H, 3.20% (2.93%); N, 0.0% (0.0%). ^{1}H NMR (400 MHz, d_3-ACN, 298 K): δ 7.87 (-$C_6\underline{H}_4$-), 7.58 (-O$\underline{H}$), 6.86 (-$C_6\underline{H}_4$-), 2.30 (br, $\underline{H}_2O$), 1.94 (CH_3CN).

U-1, $U_6O_4(OH)_4(4\text{-}HB)_{12}(H_2O)_6\cdot 12(H_2O)$, was synthesized in a nitrogen filled glovebox at room temperature following a synthetic procedure similar to that described for **Th-1**. A solution of UCl_4 (0.076 g, 0.2 mmol) in H_2O (2.00 g, 111 mmol) was added to a 3 mL shell vial containing 4-hydroxybenzoic acid (0.055 g, 0.4 mmol). The initial pH of the solution was 0.86. The vial was capped, vortexed for <1 min, and then left undisturbed in the glovebox. After 24 h, green block crystals along with white undissolved organic matter were observed. After 2 days, the solution (pH 0.66) was decanted and the product was washed twice with water and then with ethanol to remove unreacted organic matter. The crystals were then left under N_2 to dry. The yield based on U was 0.010 g (8.50%). The yield of **U-1** was likewise found to increase with reaction time, albeit to a lesser extent; harvesting the crystals after 3 days resulted in a yield of 12.8% (0.015 g) based on U. Elemental Anal. Calcd (obs): C, 27.63% (27.71%); H, 3.55% (3.70%); N, 0.0% (0.0%).

UO_2 Nanoparticle Preparation. A synthetic procedure similar to that described above for **U-1** was used to study the effects of temperature on UO_2 nanoparticle formation. A solution of UCl_4 (0.076 g, 0.2 mmol) in a 50/50 H_2O/ACN mixture (2 mL) was added to a 5 mL screw-cap vial containing 4-hydroxybenzoic acid (0.055 g, 0.4 mmol). The vial was capped and sealed with parafilm, and the reactants were vortexed for <1 min. The reaction solution was then heated at 100 °C for 24 h. The vial was removed from heat and allowed to cool for 1 h. UO_2 nanoparticles were then separated from the reaction solution by first diluting 1 mL of the heated solution in 10 mL of nanopure water. The diluted solution was then centrifuged for 1 h at 14500 rpm and 18 °C, resulting in the formation of two layers. A lighter clear green solution was removed from a dark blackish-green solution. The dark blackish-green solution, containing the UO_2 nanoparticles, was then drop-casted onto a sample holder for analysis by powder X-ray diffraction.

X-ray Structure Determination. Single crystals were selected from the bulk samples and mounted on MiTeGen micromounts in mineral oil. Reflections were collected at 100 K on a Bruker D8 QUEST diffractometer equipped with a CMOS detector using Mo Kα radiation (λ = 0.71073 Å). The data were integrated and corrected for absorption using SAINT[30,31] and a multiscan technique in SADABS,[32] included in the APEX2 crystallographic software package.[33] The structures were determined using SHELXT and refined by full-matrix least squares on F2 using the SHELXL[34] software in SHELXle.[35] Structural models of **Th-1** and **U-1** consisting of the ligand-decorated hexanuclear core as well as 12 solvent water molecules (per formula unit) were developed; however, the positions of the solvent water molecules were poorly determined. As a result, a second model was refined with contributions from the solvent water molecules removed from the diffraction data using the bypass procedure in PLATON.[36] The electron count from the "squeezed" model converged in good agreement with the number of water molecules found during the refinement of **Th-1** and **U-1**. The squeezed data are reported.

DOI: 10.1021/acs.inorgchem.8b00919
Inorg. Chem. 2018, 57, 7259−7269

Crystallographic information for these compounds can be found in Table 1.

Table 1. Crystallographic Structure Refinement Details for Th-1 and U-1 (100 K)[a]

	Th-1	U-1
formula	$Th_6C_{84}H_{76}O_{50}$	$U_6C_{84}H_{76}O_{50}$
MW (g/mol)	3277.68	3313.62
temperature (K)	100(2)	100(2)
crystal system	trigonal	trigonal
space group	$R\bar{3}c$	$R\bar{3}c$
λ (Å)	0.71073	0.71073
a (Å)	21.449(1)	21.369(4)
b (Å)	21.449(1)	21.369(4)
c (Å)	38.255(2)	38.300(8)
α (deg)	90	90
β (deg)	90	90
γ (deg)	120	120
volume (Å^3)	15242(2)	15146(6)
Z	6	6
ρ (g/cm^3)	2.143	2.180
μ (mm^{-1})	8.843	9.684
R_1	0.0290	0.0364
wR_2	0.1220	0.1613
GOF	1.062	1.491
CCDC	1579521	1579522

[a]The formula and formula weight reported do not reflect the solvent water molecules present in the structure.

For the structures of both **Th-1** and **U-1**, the HOAr portions of the ligands were disordered over two positions; the paired O−C and C−C distances were thus restrained to be similar. The μ_3-hydroxo/oxo groups (O1 and O2) of the hexanuclear core as well as the bound water molecule (O3) were each disordered over two sites and refined accordingly. Water and coordinated hydroxyl H atoms could not be located during refinement and as such were not included in the structural model. Hydroxyl H and remaining H atoms of the ligand were placed in calculated positions. Further details of the structure refinement of **Th-1** and **U-1** are provided as Supporting Information.

Powder X-ray Diffraction. Powder X-ray diffraction (PXRD) data were collected for compounds **Th-1** and **U-1** using a Rigaku Ultima IV diffractometer (Cu Kα λ = 1.542 Å; 2θ = 3−40°). Agreement between the calculated and observed patterns (Figures S3 and S4) supported that the single crystals used for structure determination were representative of the bulk sample. UO_2 nanoparticles resulting from the temperature studies *vide supra* were confirmed through comparison of the experimental powder pattern with that reported for UO_2 [ICSD reference code 35204 (Figures S5)].

Elemental Analysis. Combustion elemental analysis (EA) was performed on a PerkinElmer model 2400 elemental analyzer. Samples (1.5−2.0 mg) were weighed into small tin capsules. The samples were run in triplicate, and the reported value is the average of three runs.

Infrared and Raman Spectroscopy. Infrared spectra of **Th-1** and **U-1** were collected on a PerkinElmer FTIR Spectrum 2 system (Figure S6). The samples were diluted with dried KBr and pressed into a pellet. Scans were collected over 400−4000 cm^{-1} with 16 scans and a 2 cm^{-1} resolution. The data were acquired using the Spectrum Quant software program. Raman spectra of single crystals of **Th-1** and **U-1** were collected on a HORIBA LabRAM HR Evolution Raman Microscope with an excitation line of 532 nm (Figure S7).

Thermogravimeteric Analysis. Thermogravimetric analysis data were collected on a TA Instruments Q50 system thermogravimetric analyzer. Samples of **Th-1** (10.088 mg) and **U-1** (9.966 mg) were weighed out into platinum pans. The temperature was held at 30 °C for 30 min to dry off excess water, and then the sample was heated to 600 °C at a rate of 5 °C min^{-1} under flowing nitrogen (10 mL min^{-1}). The software TA universal analysis was used to collect and process the data (Figures S12 and S13).

Magnetic Studies. Magnetic data were collected for **U-1** on a Quantum Design Magnetic Property Measurement System (MPMS-7). Temperature-dependent data were collected under applied 1 T DC fields from 2 to 300 K, and field-dependent data were recorded at 2 K with varying applied magnetic field strengths ranging from 0 to 7 T. Corrections for the intrinsic diamagnetism of the samples were made using Pascal's constants.[37]

Solution Studies. As a means of examining the stability of the hexanuclear clusters as well as the effects of reaction time and temperature on solution speciation, a series of solutions were prepared for analysis by optical absorption spectroscopy and SAXS. However, because thorium has an [Rn]5f^0 electron configuration and is spectroscopically silent, we limited these studies to uranium for which both optical spectroscopy and SAXS could be used synergistically to elucidate solution speciation.

Reaction Time Studies. The evolution of the reaction solutions as a function of time was investigated. Solutions were prepared following the synthetic procedure outlined above for **U-1**. Aliquots of the mother liquor were collected after 1, 24, and 48 h.

Dissolution Studies. Crystals of **U-1** are insoluble in water but were readily soluble in acetonitrile. As such, the compound was dissolved in acetonitrile to examine the stability of the hexanuclear units upon dissolution.

Temperature Studies. The evolution of speciation as a function of temperature was examined for reactions prepared in a 50/50 acetonitrile/water solvent mixture. The choice of solvent systems arose from the limited solubility of the ligand in water, the observation that reaction mixtures prepared in water showed little to no scattering, and the limited solubility of UCl_4 in 100% acetonitrile. Acetonitrile/water reaction solutions were thus prepared with the molar ratios used for the preparation of **U-1**. The solutions were heated for 1 day at 25, 50, 75, and 100 °C. Aliquots of the mother liquor were subsequently collected and analyzed.

Small-Angle X-ray Scattering. All solutions were filtered (Target2 NYLON, 0.45 μm) and sealed in 1.5 mm glass capillaries (Hampton Research). Data were collected on an Anton-Paar SAXSess instrument utilizing Cu Kα radiation (λ = 1.542 Å) and line collimation. Background subtraction was performed using acetonitrile, water, or a 50/50 acetonitrile/water mixture, mirroring experimental solution conditions. SAXS data collections were 30 min in length; data were recorded over a range of 0.08−2.5 Å^{-1} on an image plate 26.1 cm from the X-ray source. SAXSQUANT software was used for data collection, treatment, and preliminary analysis (normalization, primary beam removal, background subtraction, desmearing, and smoothing). Further modeling of the SAXS data, including size distribution and PDDF analyses, was performed utilizing IRENA[38] macros within IGORPro version 6.3. A simulated scattering curve of **U-1** was calculated from SolX[39] using a structural file (xyz) derived from the single-crystal X-ray diffraction data.

Optical Absorption Spectroscopy. Optical data of the uranium(IV) solutions were collected from 400 to 700 nm on an Agilent Technologies Cary 5000 UV−vis−NIR spectrometer with a double-beam liquid attachment. The solutions were diluted by a factor of 5, and an aliquot was placed in a quartz cuvette. Solid state UV−vis−NIR data were collected for **U-1** using a Craic Technologies micro-spectrophotometer. A single crystal was paced on a quartz slide in immersion oil, and the data were collected from 300 to 1100 nm.

Dynamic Light Scattering (DLS). Dynamic light scattering data were collected for the 50/50 acetonitrile/water reaction solution that was heated at 100 °C for 24 h in an effort to further support the particle size obtained from SAXS studies. The mother liquor (1 mL) was diluted with 3 mL of a 50/50 acetonitrile/water solution to reduce the effects of multiple scattering. For an accurate hydrodynamic radius and corresponding uncertainty value, 10 separate samples were analyzed by DLS and the values were then averaged. Data were collected at room temperature using an Ar ion laser (λ = 488 nm) with a scattering angle of 90° relative to the incident beam. Scattered light was collected by a single-mode optical fiber, which was coupled to a

DOI: 10.1021/acs.inorgchem.8b00919
Inorg. Chem. 2018, 57, 7259−7269

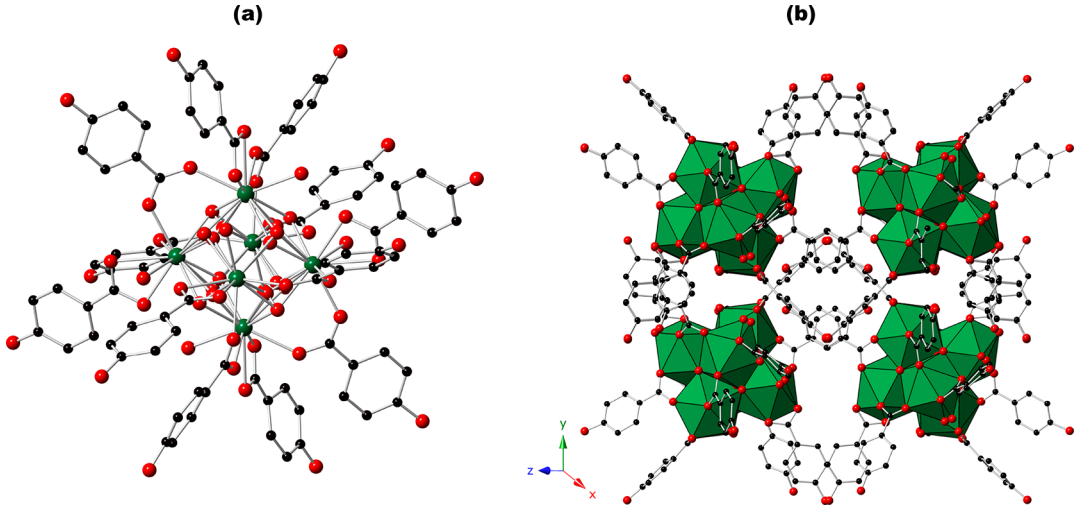

Figure 1. (a) Ball and stick representation of the ligand-decorated hexanuclear clusters that constitute **Th-1** and **U-1**. (b) Packing diagram of **U-1**. As the two compounds are isomorphous, only the U analogue is shown. Green, red, and black spheres represent uranium(IV), oxygen, and carbon atoms, respectively. Green polyhedra in panel b are nine-coordinate U(IV) metal centers. Hydrogen atoms and the disorder of the 4-HB ligands are not shown for the sake of clarity.

photon counting avalanche photodiode. The photon count rates were processed by an ALV5000 hardware autocorrelator board. The distribution of diffusion times was determined using the ALV NonLin fitting routine, a nonlinear constrained regularization of the autocorrelation function based on CONTIN, between delay times of 600 ns and 367 ms.[40] The Stokes−Einstein relation was used to convert the distribution of diffusion times to a corresponding distribution of the hydrodynamic radius, along with the viscosity of the 50/50 acetonitrile/water solution mixture of 0.81[41] and a refractive index of 1.3478.[42]

Nuclear Magnetic Resonance (NMR) Spectroscopy. Approximately 5 mg of **Th-1** was dissolved in 1 mL of d_3-ACN (concentration of ~1.5 mM). The ^{1}H NMR spectrum was obtained on a Varian MR 400 MHz spectrometer using acetonitrile as the internal reference with the chemical shift calibrated to the peak at 1.94 ppm. The ^{1}H NMR spectrum was analyzed using the MestReNova software program. The NMR spectrum is shown in Figure S8. The two peaks at 6.86 and 7.87 ppm are attributed to the ligand, while the peak at 7.58 ppm is correlated to the -OH found in the cluster core. The broad signal at 2.30 ppm is consistent with water in the cluster.[43,44]

RESULTS AND DISCUSSION

Structure Descriptions. The structures of **Th-1** and **U-1** are built from a 4-hydroxybenzoate-decorated hexanuclear $[An_6O_4(OH)_4]^{12+}$ cluster that is closely related to other ligated hexanuclear units previously reported for tetravalent metal ions, including Zr, Ce, Th, U, Np, and Pu.[12,16,17,23,45−48] For thorium and uranium, specifically, related hexanuclear clusters have been formed in the presence of both monocarboxylate (formate, acetate, chloroacetate, and glycine) and polycarboxylate (fumarate, terephthalate, 2,6-napthalenedicarboxylate, 4,4′-biphenyldicarboxylate, and DOTA) ligands.[4,9,17,49,18,24]

In the structures of **Th-1** and **U-1**, each An(IV) center is nine-coordinate, bound to four μ_3-OH/μ_3-O oxygen atoms, one bound water molecule, and four oxygen atoms from one bidentate and two monodentate 4-hydroxybenzoate ligands. As shown in Figure 1, the μ_3-OH/μ_3-O oxygen atoms are disordered over two sites. The longer An−μ_3-OH and shorter An−μ_3-O bond distances average 2.49(8) and 2.30(6) Å for **Th-1** and 2.45(7) and 2.25(5) Å for **U-1**, respectively. The An−O bond distances for the bound water molecules are slightly elongated as compared to those of the μ_3-OH/μ_3-O sites, with Th−O(H_2) and U−O(H_2) distances of 2.53(3) and 2.50(5) Å, respectively. The remaining oxygen atoms are contributed from three 4-HB ligands with An−$O_{carboxylate}$ distances ranging from 2.441(4) to 2.667(4) Å for Th and from 2.38(5) to 2.66(4) Å for U. As shown in Figure 1, two of the 4-HB ligands link each metal to two adjacent metal centers within the cluster with Th···Th and U···U distances of 3.912(1) and 3.83(3) Å, respectively. Interestingly, though the hexanuclear $[An_6O_4(OH)_4]^{12+}$ unit is analogous to those previously reported for Th and U, we note that the arrangement of the ligands and the position of the water molecules in **Th-1** and **U-1** are unique to the 4-HB-decorated analogues reported here. That is, previously reported hexanuclear Th(IV) and U(IV) clusters more commonly consist of a hexanuclear unit, wherein 12 bridging ligands decorate the cluster, with four carboxylate donors linking each metal center to its four adjacent neighbors; water molecules cap the coordination sphere typically forming a square antiprism coordination geometry. By comparison, each metal center in **Th-1** and **U-1** is capped by a chelating 4-HB unit (Figure 1a). Additionally, though the ligands terminate the clusters resulting in discrete molecular units, weak $\pi-\pi$ interactions, C−H−π, and hydrogen bonding interactions further associate the ligand-decorated units into an extended supramolecular network (Figure 1b). These interaction distances were calculated using PLATON and are summarized in the Supporting Information.[50] For **Th-1** and **U-1**, C−H−π interaction distances were found to range from 3.53(2) to 3.74(3) Å and from 3.41(3) to 3.69(2) Å, respectively. Hydrogen bonding was also present between clusters, with donor−acceptor distances ranging from 2.43(4) to 3.47(6) Å for **Th-1** and from 2.28(5) to 3.27(5) Å for **U-1**, with relative hydrogen bonding strengths classified as strong to weak interactions, respectively.[51]

Synthesis. Both **Th-1** and **U-1** were synthesized from room-temperature reactions of the respective metal chloride salt and 4-hydroxybenzoic acid in water. For both thorium and uranium, the yields were found to increase with reaction time. This may be attributed to the limited solubility of 4-hydroxybenzoic acid (0.5 g/100 mL) and the slow dissolution of the ligand over time that likely limits the amount of **Th-1** or

DOI: 10.1021/acs.inorgchem.8b00919
Inorg. Chem. 2018, 57, 7259−7269

U-1 that can form over a given reaction time. In fact, for the synthesis of both **Th-1** and **U-1**, the ligand is not completely soluble, and even after 3 days, unreacted ligand remains. In an attempt to better understand the role that the availability of the ligand had on the reaction yield as well as the identity of the complexes that may exist in solution at various time points of the reaction *vide infra*, for the uranium solutions, we filtered the reaction mixtures after 1 h and determined the amount of ligand that remained undissolved. Only 12 mg (21.8%) of the ligand dissolved after 1 h. On the basis of the available ligand in solution, we suspect that if the hexamer were to exist as a fully ligand-decorated unit in solution as has been established by previous literature reports, the 4-HB-decorated hexamer could account for only ∼22% of the U in solution.

Importantly, we added no base to promote hydrolysis to obtain the oxo and hydroxyl ligands of the hexamers or to deprotonate the ligand and allow ligation to An(IV). Despite this, the hexamer formed. The effect of pH has been investigated prior and suggests a pH of >2 is required for $U(IV)_6$ self-assembly, while $Th(IV)_6$ is optimally formed at pH ∼3.[25] On the other hand, the hexamers have never been isolated without bridging ligands such as carboxylates, and the $An(IV)_2$ dimer joined by hydroxide has been noted as an important intermediate, which aggregates rapidly to hexamers upon addition of a bridging ligand.[16] While the addition of base in these experiments would both drive hydrolysis and increase the level of dissolution of the ligand, a pH of <1.5 without added base provided the optimal synthesis. This difference from prior investigations affirms the role of the bridging ligand in promoting self-assembly, by bringing metal centers into close proximity.

Optical Absorption Spectroscopy and Small-Angle X-ray Scattering Studies. Tetravalent uranium compounds display rich optical spectra that are dominated by characteristic U(IV) f−f transitions from the $^3H_4$ ground state.[7,52−55] Recently, the peaks centered between 610 and 690 nm corresponding to three electronic transitions ($^3H_4 \rightarrow {}^3P_0$, $^3H_4 \rightarrow {}^1G_4$, and $^3H_4 \rightarrow {}^1D_2$) have been used with some success to infer U(IV) solution speciation in other carboxylate ligand systems. For example, Nyman et al.[8] and Tamain et al.[17] showed that the optical spectra for solutions consisting primarily of monomeric U(IV) species have features distinctly different from those collected for solutions (or solids) known to consist predominately of hexameric units, with differences in the position, splitting, and perhaps most importantly relative intensity of the peaks indicative of the U(IV) complexes present in solution. The optical spectra observed for monomeric and hexameric units have thus become fairly diagnostic of the nuclearity of the complex.[7,52,56] For monomeric complexes, the lower-wavelength peak often has an intensity higher than that of the higher-wavelength peak as represented by the spectrum obtained for a solution of U(IV) in 1 M HCl that is expected to consist predominately of monomers (Figure 2). By comparison, the solid state spectrum for **U-1**, known to consist of hexanuclear units, exhibits a blue shift as well as considerable differences in the relative intensity of the peaks between 610 and 690 nm. Such changes are indicative, and indeed signatures, of hexanuclear units that together with small-angle X-ray scattering exemplify powerful techniques not only for probing solution speciation but also for determining the relative size, shape, and interactions between dissolved species.[8,17] These studies and results are described below.

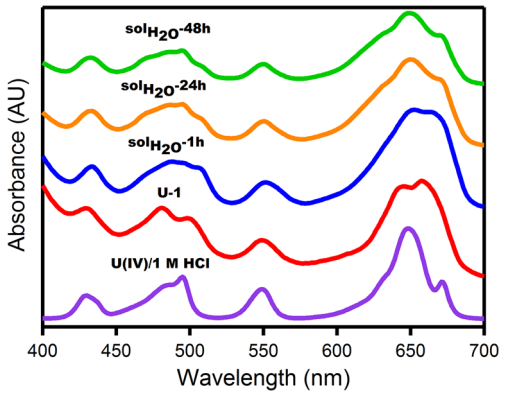

Figure 2. Optical spectra of the aqueous reaction solutions that led to the formation of **U-1** at 1 h (blue), 24 h (orange), and 48 h (green). The spectra for **U-1** (red) and U(IV) in 1 M HCl (purple) are shown for comparison.

Evolution of Reaction Solutions. The filtered aqueous reaction solution was monitored at three time intervals via SAXS and optical spectroscopy: 1, 24, and 48 h after U(IV) and 4-HBA had been combined in the reaction vial in water (denoted sol_{H_2O}-1h, sol_{H_2O}-24h, and sol_{H_2O}-48h, respectively). The optical data are presented in Figure 2. The spectrum of sol_{H_2O}-1h agrees well with the spectrum obtained for **U-1**, particularly in the region of 610−690 nm; however, it is worth noting that the spectrum is not distinctly characteristic of hexameric units for which (based on previously reported data) the ratio of the intensity of the peak centered at 654 nm to the intensity of the peak centered at 668 nm would be expected to be <1.[8] This is consistent with the limited solubility of the ligand, and the fact that if the hexamer were to exist as a fully decorated unit in solution, it can account for only roughly 22% of the total dissolved uranium. Thus, we suspect that the optical spectrum likely has contributions from multiple species in solution, one of which may include the hexamer. With time, there is a clear evolution of the absorption bands. Notably, the spectra obtained for sol_{H_2O}-24h, sol_{H_2O}-48h exhibit absorption bands that are more consistent with those characteristic of lower-nuclearity (e.g., monomeric) complexes. These data are consistent with the observation that after 24 h **U-1** is observed as a crystalline phase and hence hexameric units may no longer exist at appreciable concentrations in solution.

Soluble species in these systems were also examined using SAXS. Scattering curves for the reaction solutions (sol_{H_2O}-1h, sol_{H_2O}-24h, and sol_{H_2O}-48h) were collected and compared to the simulated curve of **U-1** as shown in Figure 3. The experimental scattering curves of the reaction solutions exhibit a relatively low scattering intensity, indicating that the solution phase species are smaller than the expected hexanuclear units. The simulated scattering curve is generated from the **U-1** solid state structure, using SolX. If the hexameric clusters were present to an appreciable extent in solution, we would expect the experimental and simulated scattering curves to closely match, particularly in the Guinier region (0.1−1.0 $Å^{-1}$), where considerable structural information can be recorded.[57] An increasing reaction time for the uranium/4-hydroxybenzioc acid systems leads to a decrease rather than an increase in scattering intensity. At 1 h, there is a distinct Guinier region between q values of 0.5 and 0.7 $Å^{-1}$, which would indicate small spherical species, i.e., hexamers or tetramers.[8,58,59] However, this feature

DOI: 10.1021/acs.inorgchem.8b00919
Inorg. Chem. 2018, 57, 7259−7269

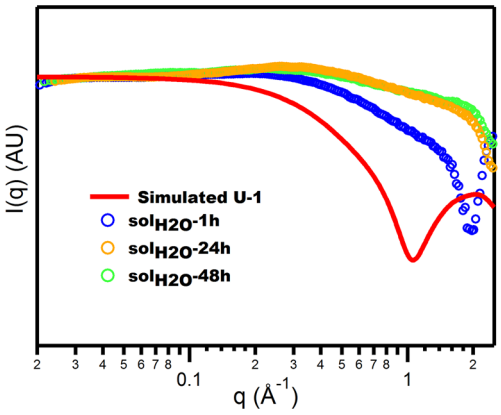

Figure 3. X-ray scattering curves of reaction solutions of **U-1** at various time intervals (1 h, blue; 24 h, orange; 48 h, green) compared to the simulated scattering curve of the hexameric structural unit of **U-1** (red). Intensity is normalized at I_0 (q = 0.018 Å^{-1}) for comparison.

is no longer apparent after 1 h. We interpret this as hexamers existing to a small extent in solution because of (1) the limited solubility of the ligand and (2) the rapid precipitation and crystallization of hexamers, both of which limit the concentration of hexamers in solution. An increasing reaction time also gives rise to a q = 1.4 Å^{-1} feature, which through the relationship $d = 2\pi/q$ is consistent with metal−metal interactions at a distance of ∼4.5 Å.[60] This feature remained present despite background subtraction and therefore can be attributed to abundant scattering species larger than a dimer, mainly metal−metal interactions given that the actinides are the strongest scatterers present in solution. The distance is slightly longer than M−M distances of ∼4.0 Å that are typically found within solid state oxo- or hydroxo-bridged oligomers.[12] However, this distance is consistent with those An···An distances found in carboxylate-bridged chains of thorium such as those described for thorium terephthalates and pyridinedicarboxylates.[6,61] An increase in the intensity of this feature illustrates an evolution of the species as a function of time. In addition, the linear slope between q values of ≈0.3 and 1.4 Å^{-1} of the reaction solutions suggests aggregation in solution. The linear feature in the scattering curves could indicate oligomeric chainlike species,[60,62] a motif that is commonly observed for actinide compounds isolated from aqueous solution in which actinide metal centers are bridged through the carboxylate ligand.[12] Similar SAXS features were recently identified and modeled as small (average of three units) bismuth sulfate chains.[63]

Taken together, the optical spectra and SAXS data point to a distribution of species that exist between lower-order ligand-bridged oligomers and hexamers. The absence of significant scattering in the reaction solutions is consistent with our hypothesis that the ligand-decorated hexamers do not exist to an appreciable extent in solution because of both the availability of the ligand that may limit the formation of the hexamer and the propensity of the ligand-decorated units to precipitate upon formation, leaving smaller oligomers in solution, which is evident in the SAXS data. This is in contrast to previous reports describing the synthesis and aqueous phase stability of An(IV) hexamers decorated by monocarboxylates such as formate, acetate, glycine, and the polycarboxylate 1,4,7,10-tetraazacyclododecane-1,4,7,10-tetraacetate (DOTA) wherein clusters could be observed in solution through various characterization techniques prior to crystallization.[8,16,25,46,64,65]

Redissolved Hexameric Units. Hexameric structural units $[AnO_4(OH)_4(H_2O)_6]^{12+}$ are well-established in the literature, having been shown to exist in the solid state and, for the monocarboxylate complexes, persist under a range of solution conditions.[6,12,16,22−27,43,46,49,64−70] Previous reports of the solution behavior of actinide hexanuclear units have shown that hexanuclear units assemble in solution prior to crystallization and remain intact upon redissolution of the crystalline product in a variety of solvents.[8,16,25,46,64,65] To further examine the effects that the ligand may have on the stability of the solution phase species, crystals of **U-1** were redissolved in acetonitrile (sol$_{ACN}$-U-1) and characterized by both optical spectroscopy and SAXS. This solvent was chosen as it is noncoordinating and therefore should not dissociate the cluster core. Additionally, crystals were not soluble in water.

The optical spectrum of sol$_{ACN}$-U-1 displays characteristic U(IV) f−f transitions from the $^3H_4$ ground state and exhibits absorption bands similar to those found in the spectrum obtained from crystals of **U-1** (Figure 4).[7,52−55] However, like the optical spectrum obtained for sol$_{H_2O}$-1h, the peaks are not distinctly characteristic of the hexanuclear units as described in previous reports.

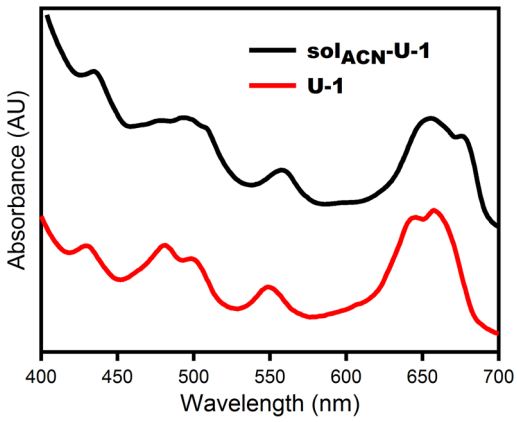

Figure 4. Optical spectra of a single crystal of **U-1** (red) and **U-1** dissolved in acetonitrile (black).

Experimental X-ray scattering curves were compared to the simulated scattering curves, shown in Figure 5. Qualitatively, the experimental scattering curve for sol$_{ACN}$-U-1 resembles the general shape of the simulated hexameric structural unit. However, the Guinier region centered at q values of 0.2−0.6 Å^{-1} for the experimental scattering curve is shifted to a lower q value, suggesting the dissolved clusters have an apparent larger radius of gyration [$R_g^2 = 3/5(Ø/2)^2$; Ø is the diameter of the spherical cluster] in an acetonitrile solution.[57,62]

Pair distance distribution function [PDDF (Figure 5b)] analysis via the Moore method[71] of simulated **U-1** and sol$_{ACN}$-U-1 provided insight. The PDDFs for both simulated **U-1** and sol$_{ACN}$-U-1 show a Gaussian distribution with a width of ∼8 Å, and additional lower-intensity distributions, where the scattering probability goes to 0 at 14 Å (simulated) and 18.5 Å (experimental). Briefly, the PDDF is a histogram of distances within the cluster, weighted by electron density contrast [i.e., electron density and probability both contribute to the vertical axis $P(r)$].[57] Often, PDDF profiles such as these are consistent with a dense core (maximum U_6 core is ∼8 Å) and a lower-

DOI: 10.1021/acs.inorgchem.8b00919
Inorg. Chem. 2018, 57, 7259−7269

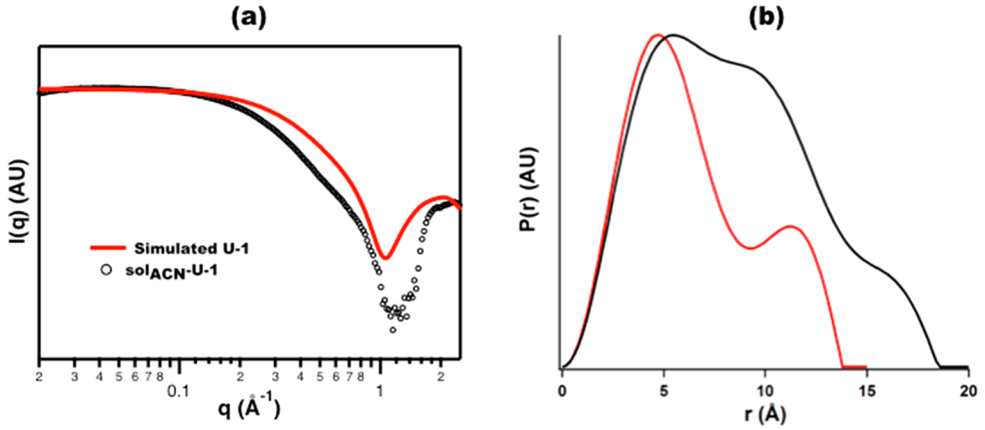

Figure 5. (a) X-ray scattering curves of **U-1** crystals dissolved in acetonitrile (black) compared to the simulated scattering curve of the hexameric structural unit (red). (b) PDDF (pair distance distribution function) derived from each scattering curve. The line color is the same as that of the scattering curves.

density shell of the hydrocarbon ligands, approximately consistent with the solid state structure. The R_g derived from the PDDF fit of the simulated **U-1** is 5.2 Å.[72] The PDDF analysis of sol$_{ACN}$-U-1 (acetonitrile) indicates larger clusters, consistent with the scattering curve (R_g = 6.2 Å). Additionally there appears to be stronger experimental scattering from the shell of the cluster where the ligands reside. Because crystals of pure **U-1** were dissolved, and we expect **U-1** to be stable in this "benign" solvent, we propose the increased scattering from the shell in the experimental data is from ordered packing of solvent molecules between the rigid ligands.

Evolution of Solution Species as a Function of Temperature. Temperature and pH are two factors that are well-known to promote hydrolysis and condensation of the actinides.[12,73] However, a limited number of studies have established the effect that the ligand may have on the transformation of lower-order oligomers to higher-order oligomers. As such, we examined solutions of U(IV) and 4-hydroxybenzoate in 50/50 H_2O/ACN solutions at 25, 50, 75, and 100 °C (denoted sol$_{H_2O/ACN}$-25, sol$_{H_2O/ACN}$-50, sol$_{H_2O/ACN}$-75, and sol$_{H_2O/ACN}$-100, respectively) using optical spectroscopy and SAXS to document the effect ligands may have on the transformation of actinide−oxo clusters with applied heat. In this case, the choice of solvent stemmed from the limited solubility of the ligand and the assembled hexamers in aqueous solution as well as the limited solubility of the UCl_4 in acetonitrile. Moreover, both the optical spectrum and the SAXS curve obtained for sol$_{H_2O/ACN}$-25 showed similarities to the data obtained from the acetonitrile solution sol$_{ACN}$-U-1, suggesting a similar distribution of species in solution.

A color change is visually observed with an increase in temperature from 25 °C; the green solution transforms to a dark green/black solution at ≥75 °C. At 100 °C, particles are clearly visible in solution. The optical spectrum was thus examined at 25 °C intervals to observe differences in the absorption bands. Both the decrease in the intensity of the characteristic peaks of U(IV) and the increase in background intensity, such as that highlighted by the spectrum obtained for sol$_{H_2O/ACN}$-100 (Figure 6), are consistent with the formation of nanometer-sized U(IV) particles or a colloidal phase.[8,74,75] The phase was confirmed to be UO_2 nanoparticles by PXRD with a particle size of 2.65 nm calculated from the Scherrer equation (Figure S5).[12,27]

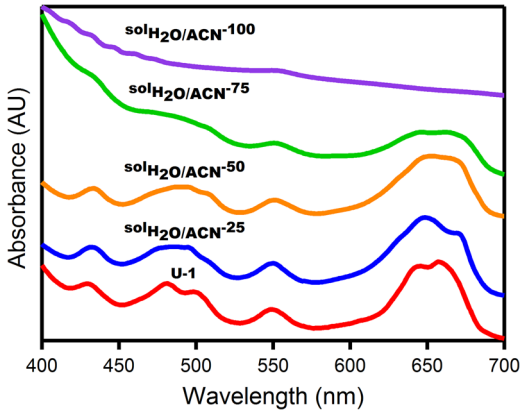

Figure 6. Transformation of the optical spectra of U(IV)/4-HBA reactions in a 50/50 H_2O/ACN solvent mixture with an increasing temperature (25 °C, blue; 50 °C, orange; 75 °C, green; 100 °C, purple). The spectrum for **U-1** (red) is shown for comparison.

To corroborate this finding, X-ray scattering curves for sol$_{H_2O/ACN}$-25, sol$_{H_2O/ACN}$-50, sol$_{H_2O/ACN}$-75, and sol$_{H_2O/ACN}$-100 were collected, and an evolution of solution species as a function of temperature was observed (Figure 7). The solution

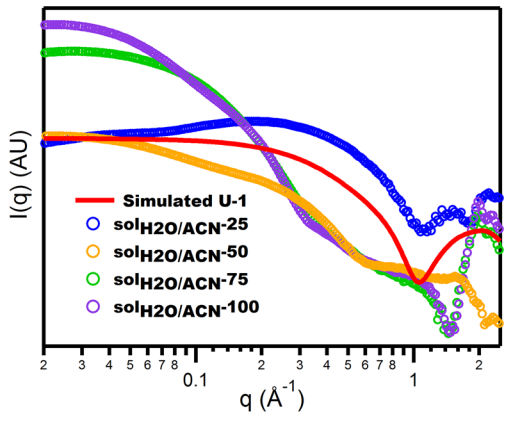

Figure 7. X-ray scattering curves of sol$_{H_2O/ACN}$-25 (blue), sol$_{H_2O/ACN}$-50 (orange), sol$_{H_2O/ACN}$-75 (green), and sol$_{H_2O/ACN}$-100 (purple). The simulated scattering curve of **U-1** (red) is shown for reference.

DOI: 10.1021/acs.inorgchem.8b00919
Inorg. Chem. 2018, 57, 7259−7269

at 25 °C exhibits a Guinier region at q values of 0.35−0.7 Å^{-1} in the scattering curve, which can be modeled via size distribution analysis (Figure S9) to have an average particle radius of 3.84 Å, slightly smaller than the simulated **U-1** radius of 4.14 Å. Interestingly, the **U-1** solution in a mixed water/acetonitrile solvent displays a Coulombic peak with a maximum intensity around 0.2 Å^{-1}, whereas the pure acetonitrile solution does not display this. This indicates clusters interact differently on the basis of solvent composition.

When the temperature of the reaction mixture is increased to 50 °C, a distinct change in the X-ray scattering curve compared to that at 25 °C is observed. At low q values (0.02−0.25 Å^{-1}), the slope is consistent with a power law dependence of approximately q^{-1} indicating a linear arrangement of particles in solution.[76] When fit with a cylindrical model, the fit matches the experimental data to yield two populations with radii of 4.43 and 7.17 Å (Figure S10). Heating to 75 and 100 °C results in a significant increase in scattering intensity at low q values in comparison to the scattering data at 50 °C. For the 75 °C solution, we fit the scattering curve between 0.02 and 0.35 Å^{-1} with a spherical model with a radius of 16.0 ± 5.8 Å, yielding a particle size of ∼32 Å (Figure S11). The curve for sol$_{H_2O/ACN}$-100 displays a scattering curve similar to the 75 °C curve, with more intense scattering at low q values as well as a slight shift of the Guinier region to low q values, indicative of larger particles. Because of the increase in the polydispersity of this sample, we were unable to provide a similar reasonable fit. Additionally, the increased linearity (instead of curved) of the region between 0.07 and 0.25 Å^{-1} suggests formation of branched superstructures of the nanoparticles which may contribute to the complexity of these scattering data.[8,76] It should be noted that sol$_{H_2O/ACN}$-75 and sol$_{H_2O/ACN}$-100 experimental scattering curves were compared to the simulated scattering curve calculated for the largest reported U(IV) cluster (U_{38}).[10] However, no consistency between the scattering curves was observed, indicating that heating **U-1** above 75 °C results in oligomeric species much larger than the U_{38} cluster.

Dynamic Light Scattering Studies. To further examine the size and distribution of particles in solution, dynamic light scattering data were collected on diluted samples (25 mM) of sol$_{H_2O/ACN}$-100. A normalized fit was obtained with a linear number-weighted distribution that showed particles with an average hydrodynamic radius of 3.8 ± 1 nm. The hydrodynamic radius corroborates the decrease in the intensity of the peaks in the optical spectrum observed for sol$_{H_2O/ACN}$-100 in Figure 6, which is attributed to the formation of a colloidal phase, as well as the size distribution of ∼3.2 nm calculated from the SAXS data. Collectively, DLS, optical spectroscopy, and SAXS revealed particles that are smaller than those of previous reports describing the transformation of glycine-decorated hexamers to particles with a radius of 6.2−8.5 nm upon heating,[8,74] which may imply that the identity of the ligand influences particle formation, with bulkier ligands stabilizing smaller particles. We also note that the DLS distribution showed a component at a larger value that is likely caused by aggregates.

Magnetic Studies. Although a number of reports have described the synthesis and structural chemistry of ligand-decorated $[An_6O_4(OH)_4]^{12+}$ hexameric units, to the best of our knowledge, the magnetic behavior of such compounds has not been extensively described. An important exception is the isopolyoxometalate cluster complex, $[Cp^{‡}_4(bpy)_2][U_6O_{13}]$ ($Cp^{‡}$ = 1,2,4-tBu$_3$C$_5$H$_2$), described by Duval, Burns, Clark, and co-workers.[77] As this complex is formed from oxidation of organometallic precursors, in this case, the average uranium oxidation state was determined to be $5f^1$ U(V) using magnetic susceptibility measurements. Variable-temperature and field-dependent magnetic measurements were thus performed to examine the magnetic properties of the polynuclear species and also confirm the uranium oxidation states in **U-1** (Figure 8). At

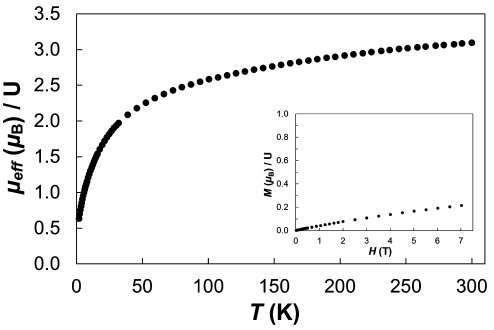

Figure 8. Variable-temperature molar magnetic data (μ_{eff}) for $U_6O_4(OH)_4(H_2O)_6(4\text{-HB})_{12}$ (per uranium cation) and variable field data collected at 2 K (inset).

room temperature, the μ_{eff} value (3.09 μ_B/U) was consistent with that expected for a U^{4+} cation.[78−81] Upon cooling, the μ_{eff} value decreased steadily to 0.63 μ_B at 2 K. The decrease in moment resulted from the depopulation of crystal field levels of the U^{4+} cations. No saturation of the magnetization in the field-dependent measurement was observed at 2 K, also characteristic of a uranium(IV) ion.[82,83] Overall, the magnetic data are consistent with the presence of six U^{4+} cations as observed in **U-1**.

Thermal Behavior. Relatively few reports have examined the thermal stability of ligand-decorated hexanuclear complexes.[9] The thermal stabilities of **Th-1** and **U-1** were thus examined over a range of 30−600 °C under flowing nitrogen. The TGA plot for **Th-1** (Figure S12) shows a total weight loss of 53% that is consistent with the decomposition of $Th_6O_4(OH)_4(H_2O)_6(4\text{-HB})_{12}\cdot nH_2O$ (n = 6) to ThO_2 (calcd 53.2%). The weight loss occurs in a series of steps, with the first weight loss of 8.4% occurring over the range of 67−127 °C. The first weight loss together with the second weight loss that is observed over the range of 127−232 °C with an additional 4.4% weight loss (total of 12.8%) is attributed to the loss of the solvent and bound water molecules as well as the -OH groups from the ligand (calcd 12.6%). Further decomposition of the ligand is then observed over a series of approximately four steps that begins at 232 °C and is complete by approximately 450 °C.

The TGA plot for **U-1** (Figure S13) collected under flowing N_2 shows a weight loss of 9.2% over the range from 50 to ∼125 °C that is consistent with the loss of the solvent and bound water molecules (calcd 9.0%) from the structure. This is immediately followed by a second transition that corresponds to a weight loss of 6% (total weight loss of 15.3%) that is consistent with the loss of the hydroxyl groups from the 4-HB ligands (calcd 15.0%). Over the range of 238−450 °C, further decomposition of the ligand, occurring in roughly four steps, is observed resulting in a total weight loss of ∼54%. The total observed weight loss (53.7%) corresponds to the decomposition of **U-1** to 6 equiv of UO_2 (calcd 54.1%). Thermal treatments under an air atmosphere of previously reported

DOI: 10.1021/acs.inorgchem.8b00919
Inorg. Chem. 2018, 57, 7259−7269

carboxylate-based compounds consisting of the hexanuclear core were found to decompose to α-U_3O_8.[9] We attribute differences in the thermal decomposition products (UO_2 vs α-U_3O_8) to the conditions under which the analyses were performed; under a nitrogen atmosphere, UO_2 is formed, whereas under air, α-U_3O_8 is observed.

CONCLUSION

Two novel An(IV) carboxylates consisting of ligand-decorated $[An_6O_4(OH)_4(H_2O)_6]^{12+}$ hexanuclear cores (An = Th and U) have been synthesized under aqueous conditions. The structures have been determined using single-crystal X-ray diffraction, and the optical, magnetic, and thermal behavior has been examined. In addition, optical spectroscopy in conjunction with small-angle X-ray scattering was used to correlate the hexanuclear units observed in the solid state to species in solution, prior to precipitation of the crystalline phase. The optical and SAXS data suggest that the hydroxybenzoate-decorated clusters do not exist to an appreciable extent in solution, which we attribute to the relatively low solubility of the ligand used in this work. However, the hexamer remained intact upon dissolution of crystals of U1 in acetonitrile. In addition, the evolution of these oligomers in acetonitrile/water solutions as a function of temperature was explored. The optical and SAXS data displayed an evolution of particle size with an increase in temperature, with the species ultimately transforming to ~3.2 nm nanoparticles at 75−100 °C as determined by SAXS, which is supported by DLS and PXRD. The results from these studies collectively point to the importance that the ligand may have on both the relative stability and the solubility of the hexanuclear units as well as their transformation to larger particles in solution. The strong ligating character of HB usurped the need to add base to drive hydrolysis and condensation from simple An(IV) monomers to hexamers. Such ligand effects and the role that substituted monocarboxylates have on complexation, precipitation, and hydrolysis and condensation processes are the subject of ongoing investigations.

ASSOCIATED CONTENT

Supporting Information

The Supporting Information is available free of charge on the ACS Publications website at DOI: 10.1021/acs.inorgchem.8b00919.

Synthesis of UCl_4, structure refinement details, powder X-ray diffraction patterns, Raman and infrared spectra, ^1H NMR spectrum, modeling fits, PDDF profiles, and TGA spectra (PDF)

Accession Codes

CCDC 1579521−1579522 contain the supplementary crystallographic data for this paper. These data can be obtained free of charge via www.ccdc.cam.ac.uk/data_request/cif, or by emailing data_request@ccdc.cam.ac.uk, or by contacting The Cambridge Crystallographic Data Centre, 12 Union Road, Cambridge CB2 1EZ, UK; fax: +44 1223 336033.

AUTHOR INFORMATION

Corresponding Author

*E-mail: kek44@georgetown.edu.

ORCID

Yusen Qiao: 0000-0001-7654-8636

Jeffery A. Bertke: 0000-0002-3419-5163

Eric J. Schelter: 0000-0002-8143-6206

May Nyman: 0000-0002-1787-0518

Karah E. Knope: 0000-0002-5690-715X

Author Contributions

N.A.V. and J.N.W. contributed equally to this work.

Notes

The authors declare no competing financial interest.

ACKNOWLEDGMENTS

This work was primarily supported by the Clare Boothe Luce Foundation and Georgetown University. E.J.S. acknowledges the U.S. Department of Energy, Office of Science, Office of Basic Energy Sciences, Separation Science program under Award Number DE-SC0017259 for financial support. The authors acknowledge Professor Jay Kikkawa (Department of Physics, University of Pennsylvania) for assistance with the magnetic measurements. The authors also gratefully acknowledge the National Science Foundation for acquisition of the Raman spectrometer and single crystal X-ray diffractometer under grants NSF CHE-1429079 and NSF CHE-1337975, respectively. The SAXS studies and analyses were performed at Oregon State University, supported by the Department of Energy, National Nuclear Security Administration under Award Number DE-NA0003763.

REFERENCES

(1) *Basic Research Needs for Environmental Management*; Office of Science, U.S. Department of Energy: Washington, DC, 2015.

(2) Thuery, P.; Harrowfield, J. Recent advances in structural studies of heterometallic uranyl-containing coordination polymers and polynuclear closed species. *Dalton Trans.* **2017**, *46* (40), 13660−13667.

(3) Andrews, M. B.; Cahill, C. L. Uranyl Bearing Hybrid Materials: Synthesis, Speciation, and Solid-State Structures. *Chem. Rev.* **2013**, *113* (2), 1121−1136.

(4) Loiseau, T.; Mihalcea, I.; Henry, N.; Volkringer, C. The crystal chemistry of uranium carboxylates. *Coord. Chem. Rev.* **2014**, *266−267*, 69−109.

(5) Novikov, A. P.; et al. Colloid Transport of Plutonium in the Far-Field of the Mayak Production Association, Russia. *Science* **2006**, *314*, 638−641.

(6) Falaise, C.; Charles, J.-S.; Volkringer, C.; Loiseau, T. Thorium Terephthalates Coordination Polymers Synthesized in Solvothermal DMF/H_2O System. *Inorg. Chem.* **2015**, *54* (5), 2235−2242.

(7) Falaise, C.; Delille, J.; Volkringer, C.; Loiseau, T. Solvothermal Synthesis of Tetravalent Uranium with Isophthalate or Pyromellitate Ligands. *Eur. J. Inorg. Chem.* **2015**, *2015* (17), 2813−2821.

(8) Falaise, C.; Neal, H. A.; Nyman, M. U(IV) Aqueous Speciation from the Monomer to UO_2 Nanoparticles: Two Levels of Control from Zwitterionic Glycine Ligands. *Inorg. Chem.* **2017**, *56* (11), 6591−6598.

(9) Falaise, C.; Volkringer, C.; Loiseau, T. Mixed Formate-Dicarboxylate Coordination Polymers with Tetravalent Uranium: Occurrence of Tetranuclear $\{U_4O_4\}$ and Hexanuclear $\{U_6O_4(OH)_4\}$ Motifs. *Cryst. Growth Des.* **2013**, *13* (7), 3225−3231.

(10) Falaise, C.; Volkringer, C.; Vigier, J.-F.; Beaurain, A.; Roussel, P.; Rabu, P.; Loiseau, T. Isolation of the Large $\{Actinide\}_{38}$ Poly-oxo Cluster with Uranium. *J. Am. Chem. Soc.* **2013**, *135* (42), 15678−15681.

(11) Zanker, H.; Hennig, C. Colloid-borne forms of tetravalent actinides. *J. Contam. Hydrol.* **2014**, *157*, 87−105.

(12) Knope, K. E.; Soderholm, L. Solution and Solid-State Structural Chemistry of Actinide Hydrates and Their Hydrolysis and Condensation Products. *Chem. Rev.* **2013**, *113* (2), 944−994.

DOI: 10.1021/acs.inorgchem.8b00919
Inorg. Chem. 2018, 57, 7259−7269

(13) Qiu, J.; Burns, P. C. Clusters of actinides with oxide, peroxide, or hydroxide bridges. *Chem. Rev.* **2013**, *113* (2), 1097−1120.
(14) Baes, C. F.; Mesmer, R. E. *The Hydrolysis of Cations*; Wiley: New York, 1976.
(15) Burgess, J. *Metal Ions in Solution*; Ellis Horwood Ltd.: Chichester, U.K., 1978.
(16) Hu, Y.-J.; Knope, K. E.; Skanthakumar, S.; Soderholm, L. Understanding the Ligand-Directed Assembly of a Hexanuclear Th^{IV} Molecular Cluster in Aqueous Solution. *Eur. J. Inorg. Chem.* **2013**, *2013* (24), 4159−4163.
(17) Tamain, C.; Dumas, T.; Hennig, C.; Guilbaud, P. Coordination of Tetravalent Actinides (An = Th^{IV}, U^{IV}, Np^{IV}, Pu^{IV}) with DOTA: From Dimers to Hexamers. *Chem. - Eur. J.* **2017**, *23* (28), 6864−6875.
(18) Falaise, C.; Assen, A.; Mihalcea, I.; Volkringer, C.; Mesbah, A.; Dacheux, N.; Loiseau, T. Coordination polymers of uranium(IV) terephthalates. *Dalton Trans.* **2015**, *44*, 2639−2649.
(19) Martin, N. P.; März, J.; Volkringer, C.; Henry, N.; Hennig, C.; Ikeda-Ohno, A.; Loiseau, T. Synthesis of coordination polymers of tetravalent actinides (uranium and neptunium) with a phthalate or mellitate ligand in an aqueous medium. *Inorg. Chem.* **2017**, *56* (5), 2902−2913.
(20) Martin, N. P.; Volkringer, C.; Falaise, C. m.; Henry, N.; Loiseau, T. Synthesis and Crystal Structure Characterization of Thorium Trimesate Coordination Polymers. *Cryst. Growth Des.* **2016**, *16* (3), 1667−1678.
(21) Volkringer, C.; Mihalcea, I.; Vigier, J.-F. o.; Beaurain, A.; Visseaux, M.; Loiseau, T. Metal−Organic-Framework-Type 1D-Channel Open Network of a Tetravalent Uranium Trimesate. *Inorg. Chem.* **2011**, *50* (23), 11865−11867.
(22) Mougel, V.; Biswas, B.; Pécaut, J.; Mazzanti, M. New insights into the acid mediated disproportionation of pentavalent uranyl. *Chem. Commun.* **2010**, *46* (45), 8648−8650.
(23) Knope, K. E.; Soderholm, L. Plutonium(IV) Cluster with a Hexanuclear $[Pu_6(OH)_4O_4]^{12+}$ Core. *Inorg. Chem.* **2013**, *52* (12), 6770−6772.
(24) Knope, K. E.; Wilson, R. E.; Vasiliu, M.; Dixon, D. A.; Soderholm, L. Thorium(IV) Molecular Clusters with a Hexanuclear Th Core. *Inorg. Chem.* **2011**, *50* (19), 9696−9704.
(25) Takao, S.; Takao, K.; Kraus, W.; Emmerling, F.; Scheinost, A. C.; Bernhard, G.; Hennig, C. First Hexanuclear U-IV and Th-IV Formate Complexes - Structure and Stability Range in Aqueous Solution. *Eur. J. Inorg. Chem.* **2009**, *2009*, 4771−4775.
(26) Nocton, G.; Pécaut, J.; Filinchuk, Y.; Mazzanti, M. Ligand assisted cleavage of uranium oxo-clusters. *Chem. Commun.* **2010**, *46* (16), 2757−2759.
(27) Biswas, B.; Mougel, V.; Pécaut, J.; Mazzanti, M. Base-Driven Assembly of Large Uranium Oxo/Hydroxo Clusters. *Angew. Chem., Int. Ed.* **2011**, *50* (25), 5745−5748.
(28) Hennig, C.; Takao, S.; Takao, K.; Weiss, S.; Kraus, W.; Emmerling, F.; Meyer, M.; Scheinost, A. C. Identification of hexanuclear Actinide(IV) carboxylates with Thorium, Uranium and Neptunium by EXAFS spectroscopy. *J. Phys.: Conf. Ser.* **2013**, *430*, 012116.
(29) Kiplinger, J. L.; Morris, D. E.; Scott, B. L.; Burns, C. J. Convenient Synthesis, Structure, and Reactivity of $(C_5Me_5)U(CH_2C_6H_5)_3$: A Simple Strategy for the Preparation of Monopentamethylcyclopentadienyl Uranium(IV) Complexes. *Organometallics* **2002**, *21*, 5978−5982.
(30) *SAINT*; Bruker AXS Inc.: Madison, WI, 2007.
(31) *APEX2*; Bruker AXS Inc.: Madison, WI, 2008.
(32) *SADABS*; Bruker AXS Inc.: Madison, WI, 2008.
(33) *APEX2*, version 2010.7; Bruker AXS Inc.: Madison, WI, 2010.
(34) Sheldrick, G. M. Crystal structure refinement with SHELXL. *Acta Crystallogr., Sect. C: Struct. Chem.* **2015**, *71* (1), 3−8.
(35) Hübschle, C. B.; Sheldrick, G. M.; Dittrich, B. ShelXle: a Qt graphical user interface for SHELXL. *J. Appl. Crystallogr.* **2011**, *44* (6), 1281−1284.
(36) Spek, A. L. PLATON SQUEEZE: a tool for the calculation of the disordered solvent contribution to the calculated structure factors. *Acta Crystallogr., Sect. C: Struct. Chem.* **2015**, *71*, 9−18.
(37) Bain, G. A.; Berry, J. F. Diamagnetic Corrections and Pascal's Constants. *J. Chem. Educ.* **2008**, *85* (4), 532.
(38) Ilavsky, J.; Jemian, P. R. Irena: tool suite for modeling and analysis of small-angle scattering. *J. Appl. Crystallogr.* **2009**, *42* (2), 347−353.
(39) Zhang, R.; Thiyagarajan, P.; Tiede, D. M. Probing protein fine structures by wide angle solution X-ray scattering. *J. Appl. Crystallogr.* **2000**, *33* (3), 565−568.
(40) Peters, R. In *Dynamic Light Scattering: The Methods and Some Applications*; Brown, W., Ed.; Clarendon Press: Oxford, U.K., 1993; pp 149−176.
(41) Thompson, J. W.; Kaiser, T. J.; Jorgenson, J. W. Viscosity measurements of methanol-water and acetonitrile-water mixtures at pressures up to 3500 bar using a novel capillary time-of-flight viscometer. *J. Chromatogr. A* **2006**, *1134* (1−2), 201−209.
(42) Bertie, J. E.; Lan, Z. Liquid Water-Acetonitrile Mixtures at 25 °C: The Hydrogen-Bonded Structure Studied through Infrared Absolute Integrated Absorption Intensities. *J. Phys. Chem. B* **1997**, *101*, 4111−4119.
(43) Vasiliu, M.; Knope, K. E.; Soderholm, L.; Dixon, D. A. Spectroscopic and Energetic Properties of Thorium(IV) Molecular Clusters with a Hexanuclear Core. *J. Phys. Chem. A* **2012**, *116* (25), 6917−6926.
(44) Gottlieb, H. E.; Kotlyar, V.; Nudelman, A. NMR chemical shifts of common laboratory solvents as trace impurities. *J. Org. Chem.* **1997**, *62* (21), 7512−7515.
(45) Hennig, C.; Ikeda-Ohno, A.; Kraus, W.; Weiss, S.; Pattison, P.; Emerich, H.; Abdala, P. M.; Scheinost, A. C. Crystal structure and solution species of Ce(III) and Ce(IV) formates: from mononuclear to hexanuclear complexes. *Inorg. Chem.* **2013**, *52* (20), 11734−11743.
(46) Takao, K.; Takao, S.; Scheinost, A. C.; Bernhard, G.; Hennig, C. Formation of Soluble Hexanuclear Neptunium(IV) Nanoclusters in Aqueous Solution: Growth Termination of Actinide(IV) Hydrous Oxides by Carboxylates. *Inorg. Chem.* **2012**, *51* (3), 1336−1344.
(47) Estes, S. L.; Antonio, M. R.; Soderholm, L. Tetravalent Ce in the Nitrate-Decorated Hexanuclear Cluster $[Ce_6(\mu_3\text{-}O)_4(\mu_3\text{-}OH)_4]^{12+}$: A Structural End Point for Ceria Nanoparticles. *J. Phys. Chem. C* **2016**, *120* (10), 5810−5818.
(48) Pan, L.; Heddy, R.; Li, J.; Zheng, C.; Huang, X.-Y.; Tang, X.; Kilpatrick, L. Synthesis and Structural Determination of a Hexanuclear Zirconium Glycine Compound Formed in Aqueous Solution. *Inorg. Chem.* **2008**, *47* (13), 5537−5539.
(49) Falaise, C.; Volkringer, C.; Vigier, J.-F.; Henry, N.; Beaurain, A.; Loiseau, T. Three-Dimensional MOF-Type Architectures with Tetravalent Uranium Hexanuclear Motifs (U_6O_8). *Chem. - Eur. J.* **2013**, *19* (17), 5324−5331.
(50) Spek, A. L. Structure validation in chemical crystallography. *Acta Crystallogr., Sect. D: Biol. Crystallogr.* **2009**, *65* (2), 148−155.
(51) Steiner, T. The hydrogen bond in the solid state. *Angew. Chem., Int. Ed.* **2002**, *41* (1), 48−76.
(52) Diwu, J.; Albrecht-Schmitt, T. E. Mixed-Valent Uranium(IV,VI) Diphosphonate: Synthesis, Structure, and Spectroscopy. *Inorg. Chem.* **2012**, *51* (8), 4432−4434.
(53) Carnall, W.; Liu, G.; Williams, C.; Reid, M. Analysis of the crystal-field spectra of the actinide tetrafluorides. I. UF_4, NpF_4, and PuF_4. *J. Chem. Phys.* **1991**, *95* (10), 7194−7203.
(54) Conway, J. G. Absorption Spectrum of UF_4 and the Energy Levels of Uranium V. *J. Chem. Phys.* **1959**, *31* (4), 1002−1004.
(55) Hashem, E.; Swinburne, A. N.; Schulzke, C.; Evans, R. C.; Platts, J. A.; Kerridge, A.; Natrajan, L. S.; Baker, R. J. Emission spectroscopy of uranium(IV) compounds: a combined synthetic, spectroscopic and computational study. *RSC Adv.* **2013**, *3* (13), 4350−4361.
(56) Wacker, J. N.; Vasiliu, M.; Huang, K.; Baumbach, R. E.; Bertke, J. A.; Dixon, D. A.; Knope, K. E. Uranium(IV) Chloride Complexes: UCl_6^{2-} and an Unprecedented $U(H_2O)_4Cl_4$ Structural Unit. *Inorg. Chem.* **2017**, *56*, 9772−9780.

DOI: 10.1021/acs.inorgchem.8b00919
Inorg. Chem. 2018, 57, 7259−7269

(57) Schnablegger, H.; Singh, Y. *The SAXS guide: Getting acquainted with the principles*; Anton Paar GmbH: Graz, Austria, 2011.
(58) Rogers, R. D.; Bond, A. H.; Witt, M. M. Macrocycle complexation chemistry 34. Polyethylene glycol and glycolate complexes of Th^{4+}. Preparation and structural characterization of $[ThCl_3(pentaethylene\ glycol)]Cl{\cdot}CH_3CN$ and the $(Th^{4+})_4$ cluster, $[Th_4Cl_8(O)(tetraethylene\ glycolate)_3]{\cdot}3CH_3CN$. *Inorg. Chim. Acta* **1991**, *182* (1), 9−17.
(59) Salmon, L.; Thuéry, P.; Ephritikhine, M. Polynuclear uranium (IV) compounds with $(\mu_3\text{-oxo})U_3$ or $(\mu_4\text{-oxo})U_4$ cores and compartmental Schiff base ligands. *Polyhedron* **2006**, *25* (7), 1537−1542.
(60) Deb, T.; Zakharov, L.; Falaise, C.; Nyman, M. Structure and Solution Speciation of U^{IV} Linked Phosphomolybdate (MoV) Clusters. *Inorg. Chem.* **2016**, *55* (2), 755−761.
(61) Kim, J.-Y.; Norquist, A. J.; O'Hare, D. $[(Th_2F_5)(NC_7H_5O_4)_2(H_2O)][NO_3]$: An Actinide−Organic Open Framework. *J. Am. Chem. Soc.* **2003**, *125* (42), 12688−12689.
(62) Nyman, M. Small-angle X-ray scattering to determine solution speciation of metal-oxo clusters. *Coord. Chem. Rev.* **2017**, *352*, 461−472.
(63) Molina, P. I.; Kozma, K.; Santala, M.; Falaise, C.; Nyman, M. Aqueous Bismuth Titanium−Oxo Sulfate Cluster Speciation and Crystallization. *Angew. Chem., Int. Ed.* **2017**, *56* (51), 16277−16281.
(64) Hennig, C.; Takao, S.; Takao, K.; Weiss, S.; Kraus, W.; Emmerling, F.; Scheinost, A. C. Structure and stability range of a hexanuclear Th(iv)-glycine complex. *Dalton Trans.* **2012**, *41* (41), 12818−12823.
(65) Tamain, C.; Dumas, T.; Guillaumont, D.; Hennig, C.; Guilbaud, P. First Evidence of a Water-Soluble Plutonium(IV) Hexanuclear Cluster. *Eur. J. Inorg. Chem.* **2016**, *2016*, 3536−3540.
(66) Berthet, J.-C.; Thuéry, P.; Ephritikhine, M. Unprecedented reduction of the uranyl ion $[UO_2]^{2+}$ into a polyoxo uranium (iv) cluster: Synthesis and crystal structure of the first f-element oxide with a $M_6(\mu_3\text{-O})_8$ core. *Chem. Commun.* **2005**, *27*, 3415−3417.
(67) Lundgren, G. The Crystal Structure of $U(OH)_2SO_4$. *Ark. Kemi* **1952**, *4* (5), 421−428.
(68) Mokry, L. M.; Dean, N. S.; Carrano, C. J. Synthesis and Structure of a Discrete Hexanuclear Uranium−Phosphate Complex. *Angew. Chem., Int. Ed. Engl.* **1996**, *35* (13−14), 1497−1498.
(69) Nocton, G.; Burdet, F.; Pécaut, J.; Mazzanti, M. Self-Assembly of Polyoxo Clusters and Extended Frameworks by Controlled Hydrolysis of Low-Valent Uranium. *Angew. Chem.* **2007**, *119* (40), 7718−7722.
(70) Zehnder, R. A.; Boncella, J. M.; Cross, J. N.; Kozimor, S. A.; Monreal, M. J.; La Pierre, H. S.; Scott, B. L.; Tondreau, A. M.; Zeller, M. Network Dimensionality of Selected Uranyl(VI) Coordination Polymers and Octopus-like Uranium(IV) Clusters. *Cryst. Growth Des.* **2017**, *17* (10), 5568−5582.
(71) Moore, P. B. Small-angle scattering. Information content and error analysis. *J. Appl. Crystallogr.* **1980**, *13* (2), 168−175.
(72) Glatter, O.; Kratky, O. *Small angle X-ray scattering*; Academic Press, 1982.
(73) Katz, J. J.; Morss, L. R.; Edelstein, N.; Fuger, J. *The Chemistry of the Actinide and Transactinide Elements*, 3rd ed.; Springer: Dordrecht, The Netherlands, 2007; Vols. *1*−*5*.
(74) Vazquez, G. J.; Dodge, C. J.; Francis, A. J. Bioreduction of U(VI)-phthalate to a polymeric U(IV)-phthalate colloid. *Inorg. Chem.* **2009**, *48* (19), 9485−9490.
(75) Priyadarshini, N.; Sampath, M.; Kumar, S.; Mudali, U. K.; Natarajan, R. A combined spectroscopic and light scattering study of hydrolysis of uranium (VI) leading to colloid formation in aqueous solutions. *J. Radioanal. Nucl. Chem.* **2013**, *298* (3), 1923−1931.
(76) Sadeghi, O.; Zakharov, L. N.; Nyman, M. Aqueous formation and manipulation of the iron-oxo Keggin ion. *Science* **2015**, *347*, 1359−1362.
(77) Duval, P. B.; Burns, C. J.; Clark, D. L.; Morris, D. E.; Scott, B. L.; Thompson, J. D.; Werkema, E. L.; Jia, L.; Andersen, R. A. Synthesis and Structural Characterization of the First Uranium Cluster Containing an Isopolyoxometalate Core. *Angew. Chem., Int. Ed.* **2001**, *40* (18), 3357−3361.
(78) Cotton, S. *Lanthanide and Actinide Chemistry*; John Wiley and Sons: West Sussex, U.K., 2006; pp 61−77.
(79) Kindra, D. R.; Evans, W. J. Magnetic susceptibility of uranium complexes. *Chem. Rev.* **2014**, *114* (18), 8865−8882.
(80) Anderson, N. H.; Odoh, S. O.; Williams, U. J.; Lewis, A. J.; Wagner, G. L.; Lezama Pacheco, J.; Kozimor, S. A.; Gagliardi, L.; Schelter, E. J.; Bart, S. C. Investigation of the electronic ground states for a reduced pyridine(diimine) uranium series: evidence for a ligand tetraanion stabilized by a uranium dimer. *J. Am. Chem. Soc.* **2015**, *137* (14), 4690−700.
(81) Castro-Rodriguez, I.; Olsen, K.; Gantzel, P.; Meyer, K. Uranium Tris-aryloxide Derivatives Supported by Triazacyclononane: Engendering a Reactive Uranium(III) Center with a Single Pocket for Reactivity. *J. Am. Chem. Soc.* **2003**, *125*, 4565−4571.
(82) Lewis, A. J.; Williams, U. J.; Kikkawa, J. M.; Carroll, P. J.; Schelter, E. J. Uranium pyrrolylamine complexes featuring a trigonal binding pocket and interligand noncovalent interactions. *Inorg. Chem.* **2012**, *51* (1), 37−39.
(83) Lewis, A. J.; Williams, U. J.; Carroll, P. J.; Schelter, E. J. Tetrakis(bis(trimethylsilyl)amido)uranium(IV): synthesis and reactivity. *Inorg. Chem.* **2013**, *52* (13), 7326−7328.

NOTE ADDED AFTER ASAP PUBLICATION

Due to a production error, this paper was published on the Web on June 7, 2018, with some of the funding information deleted from the Acknowledgment section. The corrected version was reposted on June 18, 2018.

DOI: 10.1021/acs.inorgchem.8b00919
Inorg. Chem. 2018, 57, 7259−7269